Biomacromolecules

pubs.acs.org/Biomac

Article

Close Packing of Cellulose and Chitosan in Regenerated Cellulose Fibers Improves Carbon Yield and Structural Properties of Respective Carbon Fibers

Hilda Zahra, Daisuke Sawada, Chamseddine Guizani, Yibo Ma, Shogo Kumagai, Toshiaki Yoshioka, Herbert Sixta, and Michael Hummel*

Cite This: *Biomacromolecules* 2020, 21, 4326–4335

Read Online

ACCESS | Metrics & More | Article Recommendations | Supporting Information

ABSTRACT: A low carbon yield is a major limitation for the use of cellulose-based filaments as carbon fiber precursors. The present study aims to investigate the use of an abundant biopolymer chitosan as a natural charring agent particularly on enhancing the carbon yield of the cellulose-derived carbon fiber. The ionic liquid 1,5-diazabicyclo[4.3.0]non-5-enium acetate ([DBNH]OAc) was used for direct dissolution of cellulose and chitosan and to spin cellulose–chitosan composite fibers through a dry-jet wet spinning process (Ioncell). The homogenous distribution and tight packing of cellulose and chitosan revealed by X-ray scattering experiments enable a synergistic interaction between the two polymers during the pyrolysis reaction, resulting in a substantial increase of the carbon yield and preservation of mechanical properties of cellulose fiber compared to other cobiopolymers such as lignin and xylan.

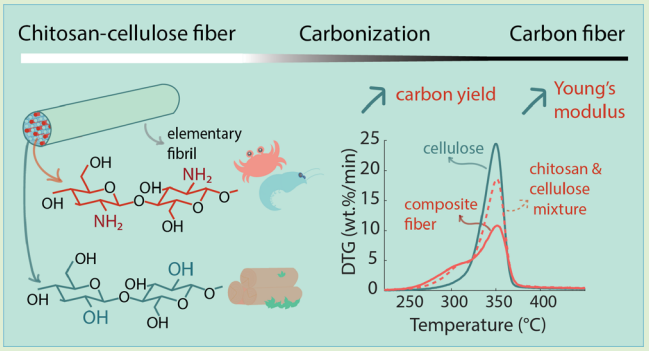

INTRODUCTION

Carbon fibers (CFs) offer a superior strength-to-weight ratio and rigidity, excellent creep resistance, and good thermal and electrical conductivities.[1] Therefore, carbon fiber-reinforced composites have found widespread use in aircrafts, automotive elements, turbine blades, construction materials, and sporting goods.[1] CFs are defined by having a carbon content of 90% or above[2] and currently produced predominantly from petroleum/coal-derived precursor fibers, namely, polyacrylonitrile (PAN) and pitch. Although PAN and pitch can produce exceptionally superior carbon fibers for high-end products, the main drawback of PAN- and pitch-based CFs is the high cost of their precursor material, which is connected to the fluctuating oil price. The slow and expensive carbonization adds further to the final price.[3] This cost structure hampers further the widespread use of CFs in the large-volume low-price market segments. Amongst other reasons, this has led to a renaissance of potentially inexpensive and renewable biopolymer-based filaments as a precursor material for CFs.

Man-made cellulosic fibers (MMCFs) have been considered as carbon fiber precursors for many decades. They can be produced from high purity and low-cost cellulosic materials with well-defined and uniform dimensions.[4] CFs from MMCFs such as Tencel or Cordenka were reported to have good strength, high thermal conductivity, and mechanical flexibility.[5−7] Although the maximum theoretical carbon yield of cellulose is 44.4 wt %,[8] the actual yield after pyrolysis can be as low as 10 wt % if no catalysts are used.[9] Amongst a series of reactions leading to volatile carbonaceous compounds, the formation of levoglucosan during cellulose pyrolysis is a main factor for the low yield.[10] This has been a major challenge in bringing the production of cellulose-based CF to the industrial scale. Strategies have been developed to suppress the formation of levoglucosan and increase the economic feasibility of cellulose-based CFs.[11] These strategies include the incorporation of various carbonization agents and were reported to improve the carbon yield up to 38 wt % (corresponding to ∼86 wt % of the theoretical carbon yield).[9,12]

Chitosan, readily available from chitin, is known to be a natural charring agent.[13,14] Its char yield upon pyrolysis has been reported to be higher than that of cellulose under the same pyrolysis condition.[15,16] Chitosan is produced on an industrial scale through enzymatic or chemical deacetylation of chitin, the second most abundant biopolymer on earth.[17,18] Its molecular structure is similar to that of cellulose except for the

Received: July 24, 2020
Revised: September 1, 2020
Published: September 1, 2020

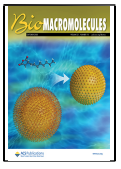

https://dx.doi.org/10.1021/acs.biomac.0c01117
Biomacromolecules 2020, 21, 4326–4335

presence of a primary amino group in the C2 position of the anhydroglucose unit.[19] This structural similarity allows blending cellulose and chitosan into a homogeneous matrix. These properties make chitosan an attractive doping agent to increase the yield of the cellulose-based CF precursor filaments without significant impairment of the mechanical property.[20] However, the dissolution of chitosan and cellulose has been challenging due to the polymer extensive intra- and intermolecular hydrogen bonds. Thus, many previous studies have employed derivatized forms of these biopolymers, which require an additional energy- and material-consuming steps in the process.[21,22] A new ionic liquid 1,5-diazabicyclo[4.3.0]non-5-enium acetate ([DBNH]OAc), which is employed in a dry-jet wet spinning process called Ioncell, is capable of dissolving cellulose without derivatization.[23,24] Moreover, Ioncell filaments possess high strength, polymer orientation, and uniformity.[23,25] These properties are highly desirable for carbon fiber precursors.[26]

For the first time, we prepare composite fibers of chitosan and cellulose through the Ioncell process, using dissolving-grade wood pulp and different types of chitosans. A facile one-stage pyrolysis of the precursor fiber without stabilization and the hot-stretching step is performed to examine the effect of chitosan incorporation on the char yield of the CF. Using extensive characterization techniques, we investigate the effect of intimately incorporated chitosan on the structural, mechanical, and thermochemical properties of the composite fiber and on the properties of the resulting CFs.

MATERIALS AND METHODS

Preparation of Chitosan−Cellulose Precursor Fibers. Birch (*Betula pendula*) prehydrolysis kraft pulp (PHK) ($[\eta]$ = 494 mL/g, M_n = 72.9 kDa, M_w = 262.9 kDa, polydispersity 3.6, Enocell Speciality Cellulose, Finland) was received from Stora Enso Enocell Mill in Finland. The cellulose was received as pulp sheets and ground to a fine powder in a Wiley mill before use. Chitosan powders were purchased from Glentham Life Science (UK), having average molecular weights of 30 kDa (CHA) and 250 kDa (CHB), respectively. The ionic liquid (IL) 1,5-diazabicyclo[4.3.0]non-5-ene-1-ium acetate ([DBNH]OAc) was synthesized from 1,5-diazabicyclo[4.3.0]non-5-ene (Fluorochem, UK) and acetic acid glacial (Merck, Germany), as described elsewhere.[25]

To prepare the chitosan−cellulose blend solution, the chitosan powder was added gradually into the IL at 75 °C and then hand-mixed thoroughly to ensure the dispersion of the chitosan powder. After that, the chitosan suspension was stirred mechanically at 30 rpm under vacuum (10−20 mbar) for 1 h at 75 °C to assure almost quantitative dissolution of chitosan. Subsequently, the ground cellulose pulp was added into the chitosan-IL solution and the resulting blend solution was continuously mixed for 2 h. All solutions were composed of 12% (w/w) of total polymer concentration and 88% (w/w) of IL. The chitosan accounted for 10% or 25% (w/w) of the total polymer concentration. As a control, a 100% cellulose solution was also prepared (12% w/w) with a similar procedure as described previously.[24] No 100% chitosan solution was prepared because such a solution would not have the viscoelastic properties needed for dry-jet wet spinning.

The viscoelastic properties of the spinning dopes were measured by Anton Paar Physica MCR 300 and MCR 302 rheometers (Austria). The complex viscosity η^* and dynamic moduli (storage modulus G', loss modulus G'') as a function of angular frequency ω were obtained through a dynamic frequency sweep test (100−0.1 s^{-1}). The apparent zero shear viscosity η_0^* was calculated by the Cross model, assuming the cellulose and chitosan−cellulose dopes follow the Cox−Merz rule.[27,28]

All solutions were spun via a dry jet-wet spinning unit (Fourné Polymertechnik, Germany) as previously described and termed Ioncell technology.[24] The take-up velocity and extrusion velocity were adjusted so that the spun fibers had draw ratios (DRs) of 2, 4, 7, and 10. The collected continuous filament was finally washed in hot water (75 °C) and air-dried throughout a continuous washing line.

Preparation of Carbon Fibers Derived from Cellulose−Chitosan Precursor Fibers. Up to 300 mg of the oven-dried precursor fiber (~10 cm length) was placed on the ceramic boat. The boat was placed inside a tubular furnace (NBD Tube Furnace) under a constant N_2 gas flow of 8.3 L/min. The temperature of the tubular furnace was increased from room temperature to the final temperature (500, 700, or 900 °C) at a 10 °C/min heating rate and then held for 30 min. After the end of the pyrolysis, the tubular furnace was allowed to reach room temperature and the boat was removed from the furnace. The weight of the carbon fiber was recorded and then compared with the weight of the precursor fiber to calculate the yield of the solid residue

$$\text{carbon yield} = \frac{w \text{ carbon fiber}}{w \text{ precursor fiber}} \times 100\% \quad (1)$$

Characterization of Precursor and Carbon Fibers. Thermal degradation of the precursor fibers was characterized by a thermogravimetric analysis (TGA) instrument (TA Instruments Q500). The initial weight of the precursor fiber was 5−10 mg. For the physical mixture of powdered cellulose fiber and chitosan powder, the experiment was conducted on a Hitachi STA7200RV. For both instruments, the measurement was carried out in an N_2 atmosphere from room temperature until 900 °C at a 10 °C/min heating rate.

The mechanical properties of the precursor fiber (tenacity, linear density, and elongation) were measured by a Favigraph tensile tester (Textechno) in a conditioned state (20 ± 2 °C and 65 ± 2 RH). The reported values are averages from 20 individual fibers. The gauge length was 20 mm, and the testing speed was 20 mm/min. The pretension weights were 100−500 mg, and the maximum forces of the load cells were 100 and 20 cN for DR 2 and DR 10, respectively. The calculation of Young's modulus was done with a Matlab script according to ASTM D2256/D2256Mf.

The mechanical properties of the carbon fibers were measured by a Universal Tester Instron 4204 100N. The single-carbon filament was fixed on a paper mounting tab with a gauge length of 20 mm. The test speed was 0.5 mm/min.

The total orientation of the precursor fibers was measured by a polarized-light microscope (Zeiss Axio Scope with a 5λ Berek compensator). The birefringence (Δn) was calculated from the division of the retardation of the polarized light by the fiber thickness, assuming a density of cellulose of 1.5 g/cm^3. The total orientation factor f_t was obtained by dividing the birefringence of the sample by the maximum value of birefringence of cellulose (0.062).[29]

The chemical functionalities of the precursor fibers were investigated by a Fourier transform infrared spectroscopy (FTIR) Nicolet6700 using a KBr method. The spectra were acquired from 64 scans, 4 cm^{-1} resolution, and wavenumber range 4000−650 cm^{-1}.

The X-ray scattering data collection, processing, and analysis were performed and are described in the Supporting Information. In short, X-ray diffraction data from the powder of the precursor fiber were collected in a transmission mode setting of a Cu Kα X-ray instrument, SmartLab (RIGAKU) operated at 45 kV and 200 mA. Collected powder diffraction data were corrected for air scattering, sample holder scattering, and inelastic scattering. The crystallinity and crystal size were estimated by a background subtraction method and Scherrer equation after a curve fitting process. The azimuthal intensity profile was obtained from the crystallographic (004) lattice plane (34.6° by 2θ) and used to estimate the Hermans orientation parameter between the fibril axis and crystallographic c axis.

Small-angle X-ray scattering (SAXS) data from the fiber samples were collected at beamline D2AM at the European Synchrotron Radiation Facility (ESRF, Grenoble, France). The X-ray energy was set to 18 keV (λ = 0.688801 Å). The data were processed correcting for the detector distortion, normalizing for the incident beam

https://dx.doi.org/10.1021/acs.biomac.0c01117
Biomacromolecules 2020, 21, 4326−4335

intensity, and subtracting the scattering contribution from air. The orientation distribution of the samples was estimated from the equatorial streak. Then, the equatorial intensity profiles of the SAXS data were obtained via azimuthal integration. The equatorial profiles of the dry samples were fitted with a power law model in the scattering vector q range of 0.007−0.06 ($Å^{-1}$), whereas the profiles of the wet samples were fitted with a WoodSAS in the q range of 0.007−0.18 using a SasView software.[30,31]

Elemental analyses of the precursor and carbon fibers were performed with a Perkin Elmer 2400 CHNS/O Analyzer. The catalytic combustion of the precursor and carbon fibers was carried out at 925 and 975 °C, respectively. The C, H, and N (wt %) contents were directly obtained from the measurement, while O (wt %) was calculated from the mass difference. Each sample was measured in duplicate.

SEM images of the precursor and carbon fibers were collected using Zeiss Sigma VP with variable pressure. To obtain clear cross-section images, the fibers should not be cut. The precursor fibers were broken by means of cryo-fracture;[25] the carbon fibers were simply pulled apart manually. Higher magnification imaging for the surface of the carbon fibers was done with a FE-SEM Hitachi S-4800. Prior to imaging, the samples were sputtered by platinum. The imaging of the precursor and carbon fibers was done at 3 and 5 kV, respectively.

RESULTS AND DISCUSSION

Spinning of Chitosan−Cellulose Precursor Fibers. Both chitosan samples dissolved readily in [DBNH]OAc. The mixed polymer solutions were translucent with a pronounced viscoelastic character. The complex viscosity of the spinning dopes was measured at various temperatures and is plotted at 70 °C in Figure 1, which corresponds to the spinning temperature. All spinning dopes, with or without chitosan, exhibited a shear thinning-like behavior where the complex viscosity decreased with higher angular frequency, suggesting a reduced entanglement between the biopolymer chains induced by the increasing shear rate.[32] The blends of cellulose pulp with the two types of chitosans showed differences in their rheological behavior. CHA had a softening effect with a gradual decrease in the complex viscosity of the solution as the share of CHA increases. By contrast, CHB induced a higher complex viscosity than CHA. The different effects of each chitosan sample are also reflected in the modulus at crossover point ($G' = G''$) in Figure S1 of the Supporting Information. An increasing share of CHA in the mixed-polymer dopes led to a noticeable reduction of the crossover modulus. The effect of CHB was more subtle. The decrease in the modulus at the crossover point suggested fewer entanglements and a less interaction between the macromolecular chains, thereby reducing the resistance to deformation.[28,33]

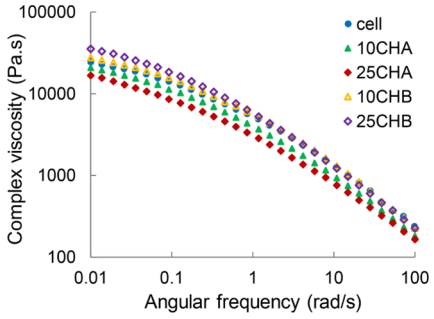

Figure 1. Complex viscosity of the spinning dopes of cellulose pulp and mixture of cellulose pulp with 10 and 25 wt % of CHA and CHB at 70 °C, respectively. All dopes had a total polymer concentration of 12 wt % in [DBNH]OAc.

The gradual decrease of both complex viscosity and crossover modulus induced by the addition of CHA was attributed to the much lower molecular weight of CHA (30 kDa) compared to the average molecular weight of the pulp cellulose used in this study (260 kDa). The molecular weight of CHB (250 kDa) is fairly close to pulp cellulose, explaining the comparable crossover modulus.[34] The minor increase in the complex viscosity is most likely due to a slightly increased interchain interaction induced by the amine and amide functional groups.[35]

Table 1 shows the rheological parameters of the cellulose and chitosan−cellulose dopes at the temperature chosen for dry-jet wet spinning. The values of the cellulose dope were within the earlier proposed optimum spinning range for cellulose dissolved in [DBNH]OAc: a zero shear viscosity of 20−30 kPa·s and a crossover modulus of 2000−4000 Pa.[36−38] Due to the thickening effect of the CHB, the spinning temperature of 25 wt % CHB was higher than for the cellulose dope to reduce the viscosity of the spin solution. As a result, the rheological parameters of the CHB-dopes were comparable to that of cellulose and a maximum draw ratio (DR) of 10 was possible, which is considered as "good spinnability".[37]

Table 1. Rheological Parameter of the Solutions of Pulp Cellulose and Mixture of Pulp and Chitosan at Different Concentrations of Chitosan Dissolved in [DBNH]OAc

dope sample	Chitosan (wt %)	total conc (wt %)	T (°C)	η_0[a] (kPa·s)	ω[b] (1/s)	$G' = G''$[c] (Pa)
cell	0	12	68	29.9	0.48	2400
10CHA	10	12	71	18.6	0.40	1500
25CHA	25	12	66	16.8	0.44	1700
10CHB	10	12	70	26.7	0.46	2400
25CHB	25	12	75	25.6	0.49	1900

[a]η_0 = zero shear viscosity. [b]ω = angular frequency at crossover point. [c]Modulus at crossover point.

The softening effect of CHA is also visible in Table 1. The CHA dopes had a noticeably lower zero-shear viscosity and crossover modulus compared to the pure cellulose dope. Despite the slightly lower rheological parameters, the CHA-containing dope also showed good spinnability demonstrated by DR 10. This deviation confirms that the optimum spinning conditions can vary depending on the type of biopolymer or biopolymer blend dissolved in the IL.[39,40]

The properties of the produced cellulose fibers and chitosan−cellulose composite fibers, including the titer, elongation, tenacity, and Young's modulus of the fibers, as a function of DR are shown in Figure S2. Overall, the results confirmed previous studies where there was a decrease in the fiber thickness or titer and elongation but an increase in the tenacity and Young's modulus of the fiber with an increasing DR.[23,41] Stretching in the air gap induces extensional stress on the extruded filament, resulting in an enhanced alignment, denser packing, and higher cohesive force between cellulose chains. Consequently, there was an increase in the chain orientation in the fiber axis and a decrease in the thickness.[23,41] The higher chain orientation contributed to the increase in the tenacity[42] and thus the Young's modulus but also caused the decrease of the elongation.[23,43] It is worth to note that the largest change in tenacity and Young's modulus occurred from

https://dx.doi.org/10.1021/acs.biomac.0c01117
Biomacromolecules 2020, 21, 4326−4335

DR 2 to DR 4. This indicated that most of the oriented structures was already formed at a moderate DR,[41,44] which was DR 4 in this study. Because of this observation, fiber samples spun at DR 4 were used to investigate the effect of chitosan incorporation on the properties of the precursor fibers and carbon fibers and for the pyrolysis study. Another consideration was that DR 4 fibers were considerably thicker than those at higher DRs. This could be beneficial to compensate for the mass loss or shrinkage during the pyrolysis process due to the formation of volatiles.

Effect of Chitosan on Structural and Mechanical Properties of the Precursor Fibers. Extrusion and coagulation of a homogeneous solution of several biopolymers do not necessarily yield a homogeneous mixed-polymer matrix. Upon coagulation, insufficient compatibility of the polymeric solutes might lead to phase separation, forming discontinuous structures with local domains consisting predominantly of the minor-share polymer. This affects the structural and mechanical properties of the resulting filaments.[35,45,46]

Table 2. Structural Properties of the Cellulose and Chitosan−Cellulose Precursor Fibers Spun at DR 4 Measured by XRD and Birefringence

	XRD			birefringence
samples	crystallite size (Å)	crystallinity (%)	Hermans parameter	total orientation
cell	31.8	35.0	0.79 ± 0.005	0.69 ± 0.04
10CHA	30.3	34.5	0.79 ± 0.006	0.69 ± 0.08
25CHA	28.9	33.3	0.80 ± 0.003	0.67 ± 0.03
10CHB	31.0	34.6	0.78 ± 0.004	0.69 ± 0.10
25CHB	26.9	31.5	0.81 ± 0.003	0.69 ± 0.11

Tables 2 and 3 summarize the structural and mechanical properties of the cellulose and the cellulose−chitosan precursor fibers, respectively. The addition of 10 wt % chitosan did not result in a notable change in the structural parameters of the cellulose fiber and thus the mechanical properties of the resulting fibers. At 25 wt %, the CHA and CHB caused a small reduction in the crystallinity and crystallite size. However, the crystalline orientation parameter measured by XRD and the total orientation determined via birefringence were unchanged even at the addition of 25 wt % chitosan (Table 2). The crystalline parameters such as crystallinity, crystallite sizes, and orientation are decisive for the tenacity of the fibers in the conditioned state.[42] Therefore, the decrease in the crystallinity by the addition of chitosan was mostly responsible for the lower tenacity of the fibers containing 25 wt % CHA or CHB compared to the reference cellulose fiber.[47−49]

The decrease in the tenacity of Ioncell cellulose fibers with the incorporation of additives, such as lignin and xylan, has been reported previously.[25,40] With the addition of 10 wt % organsolv and kraft lignin, the tenacity of the cellulose fiber decreased by 12 and 8%, respectively.[25] At 20 wt % xylan and lignin, the tenacity decreased even by 26 and 32%, respectively.[25,40] In the case of chitosan addition, the reduction of the tenacity of the cellulose composite fiber is generally lower: ∼1% with the addition of 10 wt % CHA and CHB and ∼13% with the addition of 25 wt % CHA and CHB, respectively. Furthermore, the Young's modulus of the cellulose fibers was not affected despite the addition of chitosan, which is in good agreement with other studies involving cellulose and chitosan blends,[49,50] suggesting good compatibility of cellulose and chitosan in its composite form.[50,51] Perpetuating the mechanical properties of the precursor filament despite the addition of a secondary polymer is of high importance when targeting carbon fiber production.[26] From this perspective, chitosan is an attractive copolymer for bio-based carbon fibers.

To study the macromolecular structure of the chitosan−cellulose system in more details, SAXS analyses were performed for the 10 wt % chitosan−containing filaments (Table 4). Regenerated cellulose fibers adopt a multilevel hierarchical structure.[52] SAXS can provide information regarding the nanometric structure level, which includes an elementary fibril structure consisting of crystalline and amorphous cellulose[53] and a microvoid structure between fibrils.[54] The orientation parameters of the crystals and microvoids with and without the addition of 10% CHA and CHB were similar. This means that the presence of chitosan molecules did not significantly alter the structure formation of the regenerated cellulose fiber. By contrast, polymers with a more hydrophobic character like lignin were found to phase-separate and form microdomains, which resulted in a severe decrease in the mechanical properties, as previously discussed.[25]

Table 4. Structural Parameters from Synchrotron SAXS Experiments

	dry		wet
samples	microvoids orientation	PL_exp[a]	radius of elementary fibrils (Å)
cell	0.94 ± 0.00	3.91 ± 0.004	18.5 ± 0.2
10CHA	0.91 ± 0.02	3.98 ± 0.092	20.0 ± 0.3
10CHB	0.93 ± 0.02	4.08 ± 0.002	18.9 ± 0.2

[a]Power law exponent (details can be found in Figure S3 and Table S2 of the Supporting Information).

In the equatorial profile of dry SAXS data (Figure S3), only the power law scattering was observed down to 0.007 $Å^{-1}$. This scattering is generated from surface scattering of microvoids between fibrils. Both cellulose and chitosan samples had a

Table 3. Mechanical Properties of the Cellulose and Chitosan−Cellulose Precursor Fibers Spun at DR 4 and Measured in Conditioned State

samples	titer (dtex)	diameter (μm)	elongation (%)	tenacity (cN/tex)	Young's modulus (GPa)	modulus of toughness (MPa)
cell	3.2 ± 0.3	16.6 ± 0.8	12.9 ± 1.4	41.9 ± 3.1	20.8 ± 1.5	52.8 ± 7.5
10CHA	3.1 ± 0.3	16.2 ± 0.9	11.8 ± 1.3	39.8 ± 2.9	23.4 ± 1.7	46.5 ± 8.4
25CHA	3.3 ± 0.4	16.7 ± 0.9	10.8 ± 0.7	36.4 ± 2.1	21.1 ± 1.9	37.0 ± 4.8
10CHB	3.2 ± 0.4	16.4 ± 1.0	13.2 ± 1.2	41.4 ± 2.9	22.2 ± 1.3	52.5 ± 8.5
25CHB	3.1 ± 0.3	16.3 ± 0.9	10.9 ± 1.4	36.2 ± 2.5	21.6 ± 1.0	37.9 ± 7.0

https://dx.doi.org/10.1021/acs.biomac.0c01117
Biomacromolecules 2020, 21, 4326−4335

power law exponent of approximately 4, which indicates a smooth surface of microvoids. Hence, chitosan seems to be homogeneously incorporated into the cellulose matrix and does not disorganize the cellulose fibril surface. The wet fibers produced very different scattering profiles at the high-q region (Figure S3). The difference of dry and wet data could be explained by the change of scattering contrast between structural phases like in native wood lignocellulose.[55] In the case of wood, the presence of micro-order cleavages in the cell wall produce power law scattering in the low-q region. The size and interference of elementary fibrils in the matrix of lignin and hemicellulose give rise to the scattering intensity of a cylindrical form factor combined with an interference function in the high-q region. These scattering contributions could be adjusted by the water sorption in the cleavages. Similarly, when microvoids of regenerated cellulose fibers are filled by water, the enhanced scattering contribution of wet samples at high q can be considered as scattering induced by elementary fibrils. For this reason, the equatorial profile of wet SAXS data was fitted with a WoodSAS model (the fitting details are available in the Supporting Information, Figure S3 and Table S2).[30] The elementary cylindrical radius was estimated to be approximately 2 nm for cellulose and chitosan-composite fibers, and it was in a comparable range with the XRD-derived crystallite size considering the Scherrer equation only provides a lower bound of the crystal size. A small decrease observed in the crystallite size obtained by XRD might be because of the increase of crystalline defects due to the presence of intracrystalline chitosan molecules since SAXS showed no decrease of the cylindrical diameter.

Our SAXS experiments did not show significant differences for cellulose and 10% chitosan composite fibers. In other words, there was no evidence of phase separation due to the presence of chitosan, and it is likely that chitosan chains co-crystallize with the cellulose chains. This direct association of chitosan and cellulose is the reason for the high tenacity values compared to other cellulose composite fibers and probably generates the synergetic effect for the CF production in a more efficient manner as discussed in the next section.

Effect of Chitosan on the Carbon Yield and Thermal Degradation of the Precursor Fibers. The low carbon yield during pyrolysis of cellulose is a central problem in the production of cellulose-based CFs. A yield increase is possible through uneconomically slow heating rates or impregnation with catalysts to suppress the formation of volatile carbonaceous compounds. In most cases, Lewis acids or bases are used to promote dehydration reactions.[4] The amino group in chitosan can act as such a catalyst. The homogeneous incorporation of chitosan in the cellulose matrix described in the previous chapter should enable a notable catalytic effect.

Figure 2 shows the results of the TGA measurements up to 900 °C for the precursor fibers with varying amounts of chitosans, all spun at DR 4. The addition of 10 and 25 wt % CHB increased the carbon yield by 85 and 135%, respectively. CHA gave a similar increase in carbon yields when increasing the chitosan concentration, but the carbon yield was approximately 3 wt % lower compared to CHB at the concentrations of 10 and 25 wt %.

The increase in the carbon yield upon the addition of chitosan itself was not yet a proof for any catalytic activity of chitosan during cellulose pyrolysis because chitosan has an intrinsically higher carbon yield compared to cellulose under the same pyrolysis condition.[16,56] Pyrolysis of pure CHA and

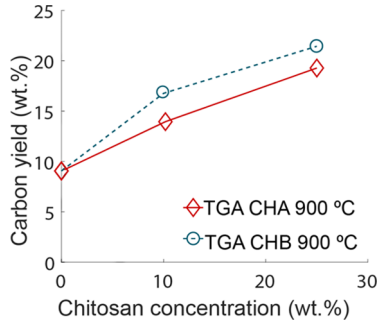

Figure 2. Carbon yield (wt %) of the cellulose fiber and composite fibers with different chitosan concentrations spun at DR 4 measured via TGA.

CHB powder resulted in a carbon yield of ∼34 wt % while the cellulose pulp gave only ∼10 wt %. However, the carbon yields were higher than expected when by simply adding the weighted yield of each single constituent. If the two biopolymers would not interact during the pyrolysis, the carbon yield and respective TG curve could be predicted by a simple weighted sum[57]

$$\mathrm{TG(T)_{add.law}} = \%\mathrm{cellulose} \times \mathrm{TG(T)_{cellulose}} + \%\ \mathrm{chitosan} \times \mathrm{TG(T)_{chitosan}} \quad (2)$$

$$\mathrm{DTG(T)_{add.law}} = \%\mathrm{cellulose} \times \mathrm{DTG(T)_{cellulose}} + \%\ \mathrm{chitosan} \times \mathrm{DTG(T)_{chitosan}} \quad (3)$$

Figure 3a,b shows the experimental TG and DTG curves of the CHA−cellulose composite fibers, individual constituents,

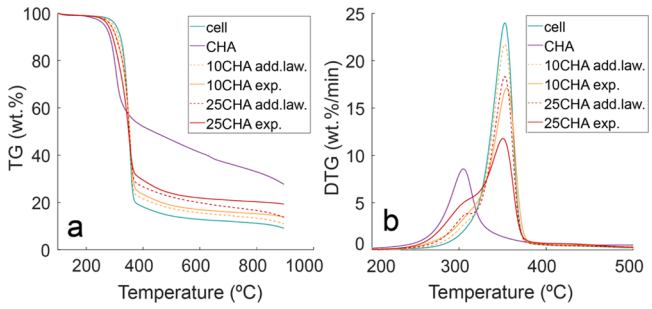

Figure 3. (a) Comparison of experimental TG curves with the corresponding additive models of cellulose and CHA-containing fibers spun at DR 4. (b) Comparison of experimental DTG curves with the corresponding additive models of cellulose and CHA-containing fibers spun at DR 4.

and calculated weighted sums (the same data for CHB are available in the Supporting Information, Figure S4). The carbon yield of the composite fibers was consistently higher than the additive values. Importantly, the experimental DTG curves show that the higher chitosan concentration led to a lower rate of the cellulose degradation peak. The rate (wt %/min) of cellulose degradation at the peak maximum decreased by ∼51 and ∼53% with the addition of 25 wt % CHA and CHB, respectively, compared to the pure cellulose fiber. This indicates that there was a notable interaction between chitosan and cellulose in the composite fiber, which altered the degradation pathways of cellulose molecules during pyrolysis.

https://dx.doi.org/10.1021/acs.biomac.0c01117
Biomacromolecules 2020, 21, 4326−4335

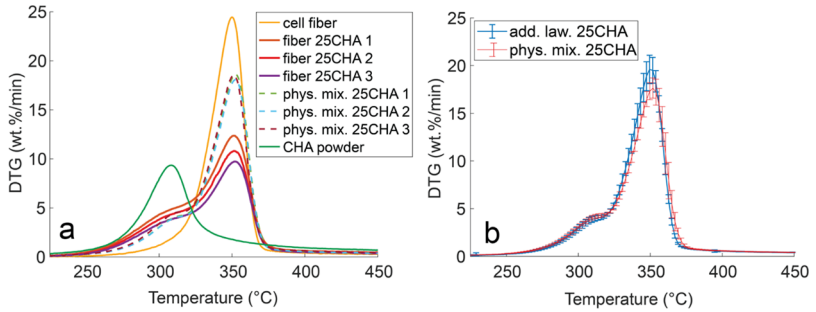

Figure 4. (a) Comparison of DTG curves of the powdered cellulose fiber, 25 wt % CHA composite fiber, the physical mixture of powdered cellulose fiber and 25 wt % CHA powder and CHA powder (numbers of 1, 2, and 3 indicate replication). (b) Comparison of DTG curves of the physical mixture and corresponding calculated curve at 25 wt % CHA addition (error bar indicates standard deviation from 5 replications).

To elucidate the catalytic effect of chitosan in the fiber matrix, the DTG curve of the composite fiber containing 25 wt % CHA was compared to the physical mixture of CHA powder and powdered cellulose fiber at the same concentration (Figure 4a). In this way, the effects of residual ionic liquid in the fibers[58,59] or the difference in the cellulose polymorphs in pulp (cellulose I) and regenerated fiber (cellulose II)[60] on the thermal degradation could be excluded. It was found that the rate at the peak maximum (wt %/min) of cellulose degradation of the 25 wt % CHA composite fibers was significantly lower than that of physical mixture (11.0 ± 1.3 vs 18.0 ± 0.50). In addition, the peak area of DTG calculated from 200 to 500 °C of the composite fiber was lower than the physical mixture, in comparison to the powdered cellulose fiber (~75 vs ~90%, respectively). Moreover, there was a difference in the shape of the chitosan degradation curve where the composite fibers had a broader shoulder than the physical mixtures.

The DTG curve of the physical mixture of the powdered cellulose fiber and chitosan powder was then compared with the corresponding curves calculated through the addition of the single components (Figure 4b). Both curves superimposed within the experimental errors. This indicates that there was no interaction between cellulose and chitosan in a mere physical contact and that the higher relative yield observed with the physical mixture (Figure 4a) was simply due to the lower amount of cellulose in the mixture. By contrast, the dissolution of chitosan and cellulose in the ionic liquid and subsequent regeneration as the homogeneous matrix resulted in a synergistic interaction between the two polymers.

The analyses on the thermal degradation above suggests that the intimate contact between cellulose and chitosan in the Ioncell fibers plays an important role in the synergistic interaction between the two biopolymers, as there was no interaction exhibited by the simple physical mixture. This interaction was likely facilitated by the amino groups in chitosan, which are known to be catalytic sites.[61] The N-functionalities in the fibers were clearly visible by FTIR (Figure S5). The band at ~1590 cm^{-1} resulting from the N−H bending vibration modes of amine and amide II groups[62] was found in all chitosan composite fibers. Several studies highlighted the role of amino groups in retaining solid products during pyrolysis, such as in Nieto-Márquez et al. where they found a higher char yield upon the pyrolysis of aniline (NH_2-benzene) compared to benzene or nitrobenzene (NO_2-benzene);[63] or chars from mixture of cellulose and L-histidine compared to cellulose and L-proline, with the latter having fewer amino functionalities.[64] Likewise, a higher degree of deacetylation, or in other words, a higher content of amino groups, was reported to result in a higher char yield for chitosan than chitin and for the monomer glucosamine compared to acetylglucosamine.[65] The slightly higher N content (N/C) in the CHB-fiber compared to CHA-fiber, shown in Table S3, might explain the slightly higher carbon yield of CHB-fiber compared to that of CHA-fiber observed in the TGA experiments (Figure 2). The marginally lower N/C in the CHA-fibers could be due to the lower molecular weight of CHA, causing a higher amount of water-soluble chitosan to be lost in the coagulation bath or continuous washing line.[66] The homogenous distribution and physical proximity of the amino groups in chitosan and cellulose in the Ioncell fiber likely amplified the interaction between the two biopolymers during pyrolysis, resulting in intermediates, which were less susceptible to the formation of volatile carbonaceous components. The detailed pyrolysis mechanisms and interaction between cellulose and chitosan during pyrolysis will be investigated further in another study.

The effect of chitosan on the carbon yields observed in the TGA was confirmed by carbonization experiments using a tubular furnace at 500, 700, and 900 °C (Figure 5), keeping the same heating rate as in the TGA. This experiment was performed to compare the intermediate yields at different temperature and study the transition through elemental analysis, presented in Table S4. At all studied temperatures, the carbon yield of CHA-fibers was slightly lower than for the CHB analogues, but the difference was within experimental errors. Higher temperature (700 °C) resulted in a lower carbon yield (wt %) compared to the lower temperature (500 °C). The decrease in the carbon yield at a higher pyrolysis temperature was due to an increased release of volatile compounds (e.g., H_2O, CO, CO_2, and $C_xH_yO_z$),[67] confirmed by the significant drop in the H/C and O/C molar ratios from

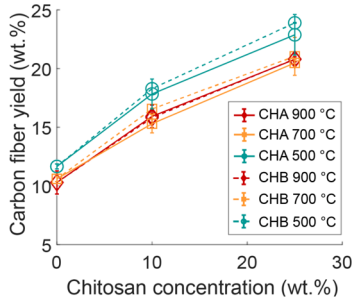

Figure 5. Carbon yield (wt %) of composite fibers with different concentrations of chitosan spun at DR 4 after oven pyrolysis.

https://dx.doi.org/10.1021/acs.biomac.0c01117
Biomacromolecules 2020, 21, 4326−4335

500 to 700 °C in Table S4. From 700 to 900 °C, the carbon yield (Figure 5) and the O/C ratio seemed to be unchanged while there was a noticeable decrease in the H/C ratio. This indicates that, at temperature higher than 700 °C, the carbon residue was already depleted of the heavy volatile compounds but still releasing hydrogen.[67] The mass loss due to the release of the hydrogen was too low to be measured in the final carbon yield at 900 °C, but it translated in a non-negligible H/C molar composition change. While the O and H contents from the original precursor fiber continuously decreased as the heat treatment progressed, the N content (N/C) first increased when the precursor fibers were pyrolyzed at 500 °C but then slightly decreased at higher temperatures. Despite that, the N/C values of the carbon fibers at 900 °C were still higher than in the precursor fiber. This suggests that the N compounds were largely retained in the carbon structure even at temperatures as high as 900 °C and the release of the N only occurred at a temperature exceeding 500 °C. The slightly higher N/C in the CHB-carbon fibers than in the CHA-carbon fibers at all pyrolysis temperatures (Table S4) was expected from the higher nitrogen content in the precursor fibers (Table S3).

Figures 6 and 7 show the cross-section and surface of the cellulose and composite precursor fibers and the resulting

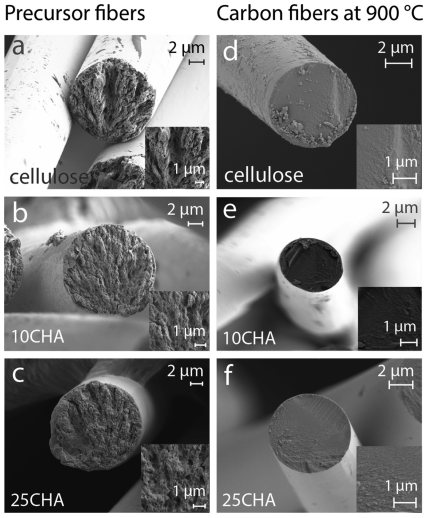

Figure 6. SEM of cross-section images of the precursor fibers of (a) cellulose, (b) 10 wt % CHA, and (c) 25 wt % CHA and carbon fibers produced at 900 °C derived from (d) cellulose, (e) 10 wt % CHA, (f) and 25 wt % CHA.

carbon fibers after heat treatment at 900 °C, respectively. All precursor fibers possessed a round cross-section and fibrillar body typical for Ioncell fibers.[25,36,41] After carbonization, the round cross-section of the original precursor fibers was still retained but the fibrillar structure disappeared and turned into a compact and dense carbon structure. Overall, the incorporation of chitosan did not alter the fiber body of the precursor and resulting carbon fibers. However, carbon fibers derived from pure cellulose had a rougher skin surface compared to the carbon fiber prepared from chitosan-containing precursor fibers. The surface roughness might be a result of recondensation of the volatiles formed during the pyrolysis of the cellulose fiber, leaving tarry deposits on the skin,[68] as shown in Figure 7d,g. As discussed previously in detail, the addition of chitosan altered the pyrolysis mechanism of cellulose. The reduced formation of larger-sized carbonaceous volatiles, and consequently less recondensation on the surface, may be one of the reasons for the smoother surface of the chitosan-derived carbon fiber in Figure 7e,f, h,i. Regarding the mechanical performance of the resulting CFs, a smooth homogeneous surface is obviously preferred as defects can be the source of mechanical failure.[69] The mechanical properties of the fibers carbonized at 900 °C are summarized in Table 5.

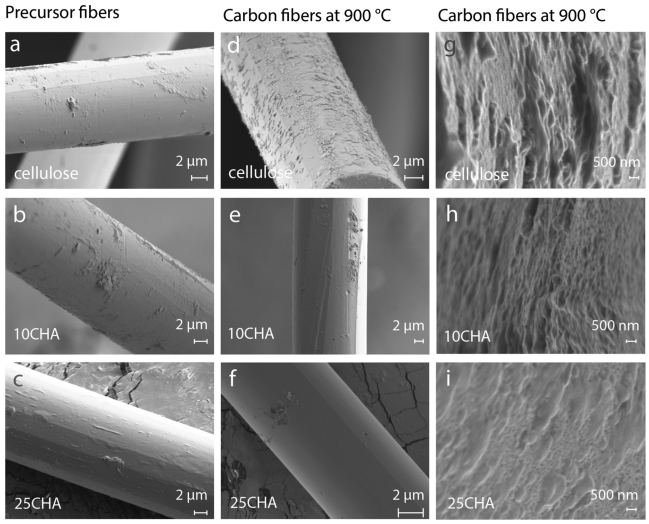

Figure 7. SEM surface images of the precursor fibers of (a) cellulose, (b) 10 wt % CHA, and (c) 25 wt % CHA and carbon fibers produced at 900 °C derived from (d, g) cellulose, (e, h) 10 wt % CHA, and (f, i) 25 wt % CHA.

Table 5. Mechanical Properties of the Carbon Fibers Obtained at 900 °C Derived from Precursor Fibers with Different Chitosan Concentrations

sample	Young's modulus (GPa)	tensile strength (MPa)
cell	20.7 ± 2.5	351 ± 63
10CHA	45.5 ± 8.3	578 ± 133
25CHA	55.3 ± 6.0	501 ± 104
10CHB	42.4 ± 3.7	361 ± 55
25CHB	29.0 ± 6.1	406 ± 156

CHA in the precursor fiber led to slightly higher tensile strengths than CHB. Also, it appeared that a higher share of chitosan was detrimental for the fiber strength. The increased carbon yield and reduction in fiber defects induced by the chitosan addition is further reflected in the increase of the Young's modulus. The carbon fibers reported herein were produced in a stationary oven at a moderate final carbonization temperature (900 °C), a relatively high heating rate (10 °C/min), and without impregnation or an additional stabilization step. The obtained Young's moduli are nevertheless comparable to values reported for other bio-based carbon fibers produced both via stationary[12,70−79] and continuous carbonization[80] or with tension applied during carbonization.[81,82] Figure 8 shows a comparison of the Young's modulus of different fibers reported in literature as a function of the final carbonization temperature. A more detailed comparison is given in the Supporting Information (Table S5). Further optimization of the heat treatment is expected to increase the mechanical properties and competitiveness of the chitosan−cellulose composite fibers of this study even further.

https://dx.doi.org/10.1021/acs.biomac.0c01117
Biomacromolecules 2020, 21, 4326−4335

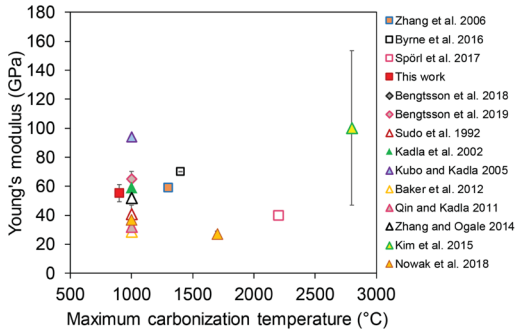

Figure 8. Comparison of the Young's modulus of 25CHA-carbon fibers in this study with carbon fibers derived from biopolymers reported by others: cellulose-based (box),[12,70,71,80] cellulose-lignin based (tilted square open),[72,73] and lignin-based (triangle up open) precursor fibers.[74−79,81,82]

CONCLUSIONS

This study provides a first assessment whether chitosan, the second most abundant biopolymer after cellulose, is suitable as a natural charring agent to improve the yield and properties of cellulose-derived carbon fiber. The pyrolysis of the hybrid bio-based fibers revealed synergetic interactions between cellulose and chitosan, resulting in a higher carbon yield and preserving the structural and mechanical properties of the fibers. When blending biopolymers, their compatibilities in the solid state upon coagulation from a homogeneous solution are mandatory to obtain even distribution and the maximum interaction between the different polymers. This shows potential to avoid impregnation of the precursor fibers with flame retardants prior to carbonization.

In the next step, we will study the interactions between the two biopolymers during the pyrolysis, to understand the reaction mechanisms and further improve chitosan/cellulose-based CFs. A further increase in the carbon yield is anticipated through optimization of the carbonization protocol. Prior to carbonization at high temperatures, pyrolysis under an oxygen or air atmosphere at low temperatures might improve the stability of the char at subsequent higher temperatures. Moreover, hot-stretching and a higher carbonization temperature (>1200 °C) as used in the continuous production of carbon fibers is expected to improve the mechanical properties of the resulting carbon fibers. These results could open up new possibilities to develop bio-based carbon fibers that can become viable alternatives for those based on nonrenewable polymers.

ASSOCIATED CONTENT

Supporting Information

The Supporting Information is available free of charge at https://pubs.acs.org/doi/10.1021/acs.biomac.0c01117.

Method of characterization of precursor fibers using XRD and SAXS, dynamic moduli of spinning dopes, mechanical properties of precursor fibers at different draw ratios, mechanical properties of precursor fibers at DR 4 in the wet state, fitting details of the precursor fibers using WoodSAS model, TG and DTG data for CHB-containing precursor fibers, FTIR spectra of CHA-containing precursor fibers, comparison of mechanical properties, and processing condition of carbon fibers derived from various precursor fibers (PDF)

AUTHOR INFORMATION

Corresponding Author

Michael Hummel − *Department of Bioproducts and Biosystems, Aalto University, Espoo 02150, Finland;* orcid.org/0000-0002-6982-031X; Email: michael.hummel@aalto.fi

Authors

Hilda Zahra − *Department of Bioproducts and Biosystems, Aalto University, Espoo 02150, Finland;* orcid.org/0000-0002-4550-9156

Daisuke Sawada − *Department of Bioproducts and Biosystems, Aalto University, Espoo 02150, Finland*

Chamseddine Guizani − *Department of Bioproducts and Biosystems, Aalto University, Espoo 02150, Finland;* orcid.org/0000-0001-7652-2751

Yibo Ma − *Department of Bioproducts and Biosystems, Aalto University, Espoo 02150, Finland*

Shogo Kumagai − *Graduate School of Environmental Studies, Tohoku University, Sendai 980-8579, Japan;* orcid.org/0000-0002-5046-372X

Toshiaki Yoshioka − *Graduate School of Environmental Studies, Tohoku University, Sendai 980-8579, Japan*

Herbert Sixta − *Department of Bioproducts and Biosystems, Aalto University, Espoo 02150, Finland;* orcid.org/0000-0002-9884-6885

Complete contact information is available at: https://pubs.acs.org/10.1021/acs.biomac.0c01117

Author Contributions

The manuscript was written through contributions of all authors. All authors have given approval to the final version of the manuscript.

Notes

The authors declare no competing financial interest.

ACKNOWLEDGMENTS

This project has received funding from the European Research Council (ERC) under the European Union's Horizon 2020 research and innovation programme (grant agreement no. 715788). The authors gratefully acknowledge: OtaNano-Nanomicroscopy Center (Aalto-NMC) for the use of XRD instrument; Graduate School of Environmental Studies (GSES) of Tohoku University for the use of the STA and FE-SEM instrument; Sauli Larkiala for the design of the sample holder for the SAXS; Dr. Isabelle Morfin for assistance at the D2AM beam line; and ESRF for the provision of beam time. HZ sincerely thanks Marja Rissanen, Kaisa Hytti, Shunsuke Kayamori for the support during tensile testing, elemental analysis and FE-SEM measurements, respectively. DS thanks Dr. Paavo Penttilä for valuable advice for the use of WoodSAS model.

REFERENCES

(1) Huang, X. Fabrication and Properties of Carbon Fibers. *Materials* **2009**, *2*, 2369−2403.

(2) Peebles, L. H., *Carbon fibers: formation, structure, and properties.* CRC Press: 2018, DOI: 10.1201/9781351070423.

(3) Park, S.-J.; Heo, G.-Y. Precursors and Manufacturing of Carbon Fibers. In *Carbon Fibers*; Park, S.-J., Ed. Springer Netherlands: Dordrecht, 2015; Vol. *210*.

(4) Frank, E.; Steudle, L. M.; Ingildeev, D.; Spörl, J. M.; Buchmeiser, M. R. Carbon Fibers: Precursor Systems, Processing, Structure, and Properties. *Angew. Chem., Int. Ed.* **2014**, *53*, 5262−5298.

(5) Wu, Q.; Pan, D. A new cellulose based carbon fiber from a lyocell precursor. *Text. Res. J.* **2002**, *72*, 405−410.
(6) Lewandowska, A. E.; Soutis, C.; Savage, L.; Eichhorn, S. J. Carbon fibres with ordered graphitic-like aggregate structures from a regenerated cellulose fibre precursor. *Compos. Sci. Technol.* **2015**, *116*, 50−57.
(7) Ogale, A. A.; Zhang, M.; Jin, J. Recent advances in carbon fibers derived from biobased precursors. *J. Appl. Polym. Sci.* **2016**, *133*, DOI: 10.1002/app.43794.
(8) Dumanlı, A. G.; Windle, A. H. Carbon fibres from cellulosic precursors: a review. *J. Mater. Sci.* **2012**, *47*, 4236−4250.
(9) Byrne, N.; Chen, J.; Fox, B. Enhancing the carbon yield of cellulose based carbon fibres with ionic liquid impregnates. *J. Mater. Chem. A* **2014**, *2*, 15758−15762.
(10) Tang, M. M.; Bacon, R. Carbonization of cellulose fibers—I. Low temperature pyrolysis. *Carbon* **1964**, *2*, 211−220.
(11) Zhou, X.; Wang, P.; Zhang, Y.; Zhang, X.; Jiang, Y. From Waste Cotton Linter: A Renewable Environment-Friendly Biomass Based Carbon Fibers Preparation. *ACS Sustainable Chem. Eng.* **2016**, *4*, 5585−5593.
(12) Spörl, J. M.; Beyer, R.; Abels, F.; Cwik, T.; Müller, A.; Hermanutz, F.; Buchmeiser, M. R. Cellulose-derived carbon fibers with improved carbon yield and mechanical properties. *Macromol. Mater. Eng.* **2017**, *302*, 1700195.
(13) Liu, X.; Gu, X.; Sun, J.; Zhang, S. Preparation and characterization of chitosan derivatives and their application as flame retardants in thermoplastic polyurethane. *Carbohydr. Polym.* **2017**, *167*, 356−363.
(14) Pan, H.; Wang, W.; Pan, Y.; Song, L.; Hu, Y.; Liew, K. M. Formation of self-extinguishing flame retardant biobased coating on cotton fabrics via Layer-by-Layer assembly of chitin derivatives. *Carbohydr. Polym.* **2015**, *115*, 516−524.
(15) Stefanescu, C.; Daly, W. H.; Negulescu, I. I. Biocomposite films prepared from ionic liquid solutions of chitosan and cellulose. *Carbohydr. Polym.* **2012**, *87*, 435−443.
(16) Jia, Y.; Wang, X.; Huo, M.; Zhai, X.; Li, F.; Zhong, C. Preparation and characterization of a novel bacterial cellulose/chitosan bio-hydrogel. *Nanomater. Nanotechnol.* **2017**, *7*, 1847980417707172−1847980417707178.
(17) Elieh-Ali-Komi, D.; Hamblin, M. R. Chitin and Chitosan: Production and Application of Versatile Biomedical Nanomaterials. *Int. J. Adv. Res.* **2016**, *4*, 411−427.
(18) van den Broek, L. A. M.; Knoop, R. J. I.; Kappen, F. H. J.; Boeriu, C. G. Chitosan films and blends for packaging material. *Carbohydr. Polym.* **2015**, *116*, 237−242.
(19) Mohammed, M. O.; Hussain, K. S.; Haj, N. Q. Preparation and Bioactivity Assessment of Chitosan-1-Acetic Acid-5-Flurouracil Conjugates as Cancer Prodrugs. *Molecules* **2017**, *22*, 1629.
(20) H.P.S, A. K.; Saurabh, C. K.; Adnan, A. S.; Nurul Fazita, M. R.; Syakir, M. I.; Davoudpour, Y.; Rafatullah, M.; Abdullah, C. K.; Haafiz, M. K. M.; Dungani, R. A review on chitosan-cellulose blends and nanocellulose reinforced chitosan biocomposites: Properties and their applications. *Carbohydr. Polym.* **2016**, *150*, 216−226.
(21) Pillai, C. K. S.; Paul, W.; Sharma, C. P. Chitin and chitosan polymers: Chemistry, solubility and fiber formation. *Prog. Polym. Sci.* **2009**, *34*, 641−678.
(22) Xu, X.; Zhuang, X.; Cheng, B.; Xu, J.; Long, G.; Zhang, H. Manufacture and properties of cellulose/O-hydroxyethyl chitosan blend fibers. *Carbohydr. Polym.* **2010**, *81*, 541−544.
(23) Sixta, H.; Michud, A.; Hauru, L.; Asaadi, S.; Ma, Y.; King, A. W. T.; Kilpeläinen, I.; Hummel, M. Ioncell-F: a high-strength regenerated cellulose fibre. *Nord. Pulp Pap. Res. J.* **2015**, *30*, 43−57.
(24) Michud, A.; Tanttu, M.; Asaadi, S.; Ma, Y.; Netti, E.; Kääriainen, P.; Persson, A.; Berntsson, A.; Hummel, M.; Sixta, H. Ioncell-F: ionic liquid-based cellulosic textile fibers as an alternative to viscose and Lyocell. *Text. Res. J.* **2015**, *86*, 543−552.
(25) Ma, Y.; Asaadi, S.; Johansson, L.-S.; Ahvenainen, P.; Reza, M.; Alekhina, M.; Rautkari, L.; Michud, A.; Hauru, L.; Hummel, M.; Sixta, H. High-Strength Composite Fibers from Cellulose−Lignin Blends Regenerated from Ionic Liquid Solution. *ChemSusChem* **2015**, *8*, 4030−4039.
(26) Gupta, A. K.; Paliwal, D. K.; Bajaj, P. Acrylic Precursors for Carbon Fibers. *J. Macromol. Sci., Part A: Polym. Rev.* **1991**, *31*, 1−89.
(27) Sammons, R. J.; Collier, J. R.; Rials, T. G.; Petrovan, S. Rheology of 1-butyl-3-methylimidazolium chloride cellulose solutions I. Shear rheology. *J. Appl. Polym. Sci.* **2008**, *110*, 1175−1181.
(28) Duan, X.; Xu, J.; He, B.; Li, J.; Sun, Y. Preparation and rheological properties of cellulose/chitosan homogeneous solution in ionic liquid. *BioResources* **2011**, *6*, 4640−4651.
(29) Adusumalli, R.-B.; Keckes, J.; Martinschitz, K. J.; Boesecke, P.; Weber, H.; Roeder, T.; Sixta, H.; Gindl, W. Comparison of molecular orientation and mechanical properties of lyocell fibre tow and staple fibres. *Cellulose* **2009**, *16*, 765−772.
(30) Penttilä, P. A.; Rautkari, L.; Österberg, M.; Schweins, R. Small-angle scattering model for efficient characterization of wood nanostructure and moisture behaviour. *J. Appl. Crystallogr.* **2019**, *52*, 369−377.
(31) Doucet, M.; Cho, J. H.; Alina, G.; Bakker, J.; Bouwman, W.; Butler, P.; Campbell, K.; Gonzales, M.; Heenan, R.; Jackson, A.; Juhas, P.; King, S.; Kienzle, P.; Krzywon, J.; Markvardsen, A.; Nielsen, T.; O'Driscoll, L.; Potrzebowski, W.; Ferraz Leal, R.; Richter, T.; Rozycko, P.; Washington, A. *SasView Version 4.1*; *Zenodo* 2017; DOI: 10.5281/zenodo.438138.
(32) Chen, X.; Zhang, Y.; Cheng, L.; Wang, H. Rheology of concentrated cellulose solutions in 1-butyl-3-methylimidazolium chloride. *J. Polym. Environ.* **2009**, *17*, 273−279.
(33) Asaadi, S.; Kakko, T.; King, A. W. T.; Kilpeläinen, I.; Hummel, M.; Sixta, H. High-performance acetylated ioncell-F fibers with low degree of substitution. *ACS Sustainable Chem. Eng.* **2018**, *6*, 9418−9426.
(34) Hou, Z.; Zhang, M.; Liu, B.; Yan, Q.; Yuan, F.; Xu, D.; Gao, Y. Effect of chitosan molecular weight on the stability and rheological properties of β-carotene emulsions stabilized by soybean soluble polysaccharides. *Food Hydrocolloids* **2012**, *26*, 205−211.
(35) Hummel, M.; Michud, A.; Tanttu, M.; Asaadi, S.; Ma, Y.; Hauru, L. K. J.; Parviainen, A.; King, A. W. T.; Kilpeläinen, I.; Sixta, H. Ionic liquids for the production of man-made cellulosic fibers: Opportunities and challenges. In *Cellulose Chemistry and Properties: Fibers, Nanocelluloses and Advanced Materials*; Springer: 2015; pp. 133−168, DOI: 10.1007/12_2015_307.
(36) Haslinger, S.; Ye, Y.; Rissanen, M.; Hummel, M.; Sixta, H. Cellulose Fibers for High Performance Textiles Functionalized with Incorporated Gold and Silver Nanoparticles. *ACS Sustainable Chem. Eng.* **2019**, *8*, 649−658.
(37) Asaadi, S.; Hummel, M.; Hellsten, S.; Härkäsalmi, T.; Ma, Y.; Michud, A.; Sixta, H. Renewable high-performance fibers from the chemical recycling of cotton waste utilizing an ionic liquid. *ChemSusChem* **2016**, *9*, 3250−3258.
(38) Ma, Y.; Hummel, M.; Kontro, I.; Sixta, H. High performance man-made cellulosic fibres from recycled newsprint. *Green Chem.* **2018**, *20*, 160−169.
(39) Haslinger, S.; Wang, Y.; Rissanen, M.; Lossa, M. B.; Tanttu, M.; Ilen, E.; Määttänen, M.; Harlin, A.; Hummel, M.; Sixta, H. Recycling of vat and reactive dyed textile waste to new colored man-made cellulose fibers. *Green Chem.* **2019**, *21*, 5598−5610.
(40) Nypelö, T.; Asaadi, S.; Kneidinger, G.; Sixta, H.; Konnerth, J. Conversion of wood-biopolymers into macrofibers with tunable surface energy via dry-jet wet-spinning. *Cellulose* **2018**, *25*, 5297−5307.
(41) Michud, A.; Hummel, M.; Sixta, H. Influence of process parameters on the structure formation of man-made cellulosic fibers from ionic liquid solution. *J. Appl. Polym. Sci.* **2016**, *133*, 43718.
(42) Krässig, H. A. Effect of structure and morphology on accessibility and reactivity. In *Cellulose: structure, accessibility, and reactivity*; Gordon and Breach Science Publishers, 1993, Vol. *11*, pp 167−324.
(43) Northolt, M. G.; Den Decker, P.; Picken, S. J.; Baltussen, J. J. M.; Schlatmann, R. The tensile strength of polymer fibres. In

https://dx.doi.org/10.1021/acs.biomac.0c01117
Biomacromolecules 2020, 21, 4326−4335

Polymeric and Inorganic Fibers; Springer: 2005; pp. 1−108, DOI: 10.1007/b104207.
(44) Asaadi, S.; Hummel, M.; Ahvenainen, P.; Gubitosi, M.; Olsson, U.; Sixta, H. Structural analysis of Ioncell-F fibres from birch wood. *Carbohydr. Polym.* **2018**, *181*, 893−901.
(45) Wendler, F.; Meister, F.; Wawro, D.; Wesolowska, E.; Ciechanska, D.; Saake, B.; Puls, J.; Le Moigne, N.; Navard, P. Polysaccharide blend fibres formed from NaOH, N-methylmorpholine-N-oxide and 1-ethyl-3-methylimidazolium acetate. *Fibres text. east. eur.* **2010**, *18*, 21−30.
(46) Wendler, F.; Persin, Z.; Stana-Kleinschek, K.; Reischl, M.; Ribitsch, V.; Bohn, A.; Fink, H.-P.; Meister, F. Morphology of polysaccharide blend fibers shaped from NaOH, N-methylmorpholine-N-oxide and 1-ethyl-3-methylimidazolium acetate. *Cellulose* **2011**, *18*, 1165−1178.
(47) Kim, J.; Cai, Z.; Lee, H. S.; Choi, G. S.; Lee, D. H.; Jo, C. Preparation and characterization of a bacterial cellulose/chitosan composite for potential biomedical application. *J. Polym. Res.* **2011**, *18*, 739−744.
(48) Isogai, A.; Atalla, R. H. Preparation of cellulose-chitosan polymer blends. *Carbohydr. Polym.* **1992**, *19*, 25−28.
(49) Hasegawa, M.; Isogai, A.; Kuga, S.; Onabe, F. Preparation of cellulose-chitosan blend film using chloral/dimethylformamide. *Polymer* **1994**, *35*, 983−987.
(50) Azevedo, E. P.; Retarekar, R.; Raghavan, M. L.; Kumar, V. Mechanical properties of cellulose: chitosan blends for potential use as a coronary artery bypass graft. *J. Biomater. Sci., Polym. Ed.* **2013**, *24*, 239−252.
(51) Ma, B.; Zhang, M.; He, C.; Sun, J. New binary ionic liquid system for the preparation of chitosan/cellulose composite fibers. *Carbohydr. Polym.* **2012**, *88*, 347−351.
(52) Schuster, K. C.; Aldred, P.; Villa, M.; Baron, M.; Loidl, R.; Biganska, O.; Patlazhan, S.; Navard, P.; Rüf, H.; Jericha, E. Characterising the emerging lyocell fibres structures by ultra small angle neutron scattering (USANS). *Lenzinger Ber.* **2003**, *82*, 107−117.
(53) Fischer, E. W.; Herchenröder, P.; Manley, R. S. J.; Stamm, M. Small-angle neutron scattering of selectively deuterated cellulose. *Macromolecules* **1978**, *11*, 213−217.
(54) Sharma, A.; Sen, D.; Thakre, S.; Kumaraswamy, G. Characterizing microvoids in regenerated cellulose fibers obtained from viscose and lyocell processes. *Macromolecules* **2019**, *52*, 3987−3994.
(55) Jakob, H. F.; Tschegg, S. E.; Fratzl, P. Hydration dependence of the wood-cell wall structure in Picea abies. A small-angle X-ray scattering study. *Macromolecules* **1996**, *29*, 8435−8440.
(56) Lin, S.; Chen, L.; Huang, L.; Cao, S.; Luo, X.; Liu, K.; Huang, Z. Preparation and characterization of chitosan/cellulose blend films using ZnCl2● 3H2O as a solvent. *BioResources* **2012**, *7*, 5488−5499.
(57) Shao, Y.; Guizani, C.; Grosseau, P.; Chaussy, D.; Beneventi, D. Thermal characterization and kinetic analysis of microfibrillated cellulose/lignosulfonate blends. *J. Anal. Appl. Pyrolysis* **2017**, *124*, 25−34.
(58) Muhammad, N.; Man, Z.; Khalil, M. A. B.; Tan, I. M.; Maitra, S. Studies on the thermal degradation behavior of ionic liquid regenerated cellulose. *Waste Biomass Valorization* **2010**, *1*, 315−321.
(59) Spörl, J. M.; Ota, A.; Son, S.; Massonne, K.; Hermanutz, F.; Buchmeiser, M. R. Carbon fibers prepared from ionic liquid-derived cellulose precursors. *Mater. Today Commun.* **2016**, *7*, 1−10.
(60) Phinichka, N.; Kaenthong, S. Regenerated cellulose from high alpha cellulose pulp of steam-exploded sugarcane bagasse. *J. Mater. Res. Technol.* **2018**, *7*, 55−65.
(61) Ali, A.; Ahmed, S. A review on chitosan and its nanocomposites in drug delivery. *Int. J. Biol. Macromol.* **2018**, *109*, 273−286.
(62) Lawrie, G.; Keen, I.; Drew, B.; Chandler-Temple, A.; Rintoul, L.; Fredericks, P.; Grøndahl, L. Interactions between alginate and chitosan biopolymers characterized using FTIR and XPS. *Biomacromolecules* **2007**, *8*, 2533−2541.
(63) Nieto-Márquez, A.; Espartero, I.; Lazo, J. C.; Romero, A.; Valverde, J. L. Direct synthesis of carbon and nitrogen−carbon nanospheres from aromatic hydrocarbons. *Chem. Eng. J.* **2009**, *153*, 211−216.
(64) Darvell, L. I.; Brindley, C.; Baxter, X. C.; Jones, J. M.; Williams, A. Nitrogen in biomass char and its fate during combustion: a model compound approach. *Energy Fuels* **2012**, *26*, 6482−6491.
(65) Qiao, Y.; Chen, S.; Liu, Y.; Sun, H.; Jia, S.; Shi, J.; Pedersen, C. M.; Wang, Y.; Hou, X. Pyrolysis of chitin biomass: TG−MS analysis and solid char residue characterization. *Carbohydr. Polym.* **2015**, *133*, 163−170.
(66) Tian, M.; Tan, H.; Li, H.; You, C. Molecular weight dependence of structure and properties of chitosan oligomers. *RSC Adv.* **2015**, *5*, 69445−69452.
(67) Liu, W.-J.; Jiang, H.; Yu, H.-Q. Development of biochar-based functional materials: toward a sustainable platform carbon material. *Chem. Rev.* **2015**, *115*, 12251−12285.
(68) Cross, C. B.; Ecker, D. R.; Stein, O. L. Artificial graphite process. U.S. Patent 3,116,975, January 7, 1964.
(69) Bascom, W. D.; Drzal, L. T. The Surface Properties of Carbon Fibers and Their Adhesion to Organic Polymers. In *NASA Technical Reports Server*; 1987.
(70) Zhang, H.; Guo, L.; Shao, H.; Hu, X. Nano-carbon black filled Lyocell fiber as a precursor for carbon fiber. *J. Appl. Polym. Sci.* **2006**, *99*, 65−74.
(71) Golova, L. K.; Makarov, I. S.; Bondarenko, G. N.; Mironova, M. V.; Berkovich, A. K.; Shandryuk, G. A.; Vinogradov, M. I.; Bermeshev, M. V.; Kulichikhin, V. G. Composite Fibers Based on Cellulose and Vinyltriethoxysilane as Precursors of Carbon Materials. *Polym. Sci., Ser. B* **2020**, *62*, 152−162.
(72) Bengtsson, A.; Bengtsson, J.; Olsson, C.; Sedin, M.; Jedvert, K.; Theliander, H.; Sjöholm, E. Improved yield of carbon fibres from cellulose and kraft lignin. *Holzforschung* **2018**, *72*, 1007−1016.
(73) Bengtsson, A.; Bengtsson, J.; Sedin, M.; Sjöholm, E. Carbon fibers from lignin-cellulose precursors: effect of stabilization conditions. *ACS Sustainable Chem. Eng.* **2019**, *7*, 8440−8448.
(74) Sudo, K.; Shimizu, K. A new carbon fiber from lignin. *J. Appl. Polym. Sci.* **1992**, *44*, 127−134.
(75) Kadla, J. F.; Kubo, S.; Venditti, R. A.; Gilbert, R. D.; Compere, A. L.; Griffith, W. Lignin-based carbon fibers for composite fiber applications. *Carbon* **2002**, *40*, 2913−2920.
(76) Baker, D. A.; Gallego, N. C.; Baker, F. S. On the characterization and spinning of an organic-purified lignin toward the manufacture of low-cost carbon fiber. *J. Appl. Polym. Sci.* **2012**, *124*, 227−234.
(77) Kubo, S.; Kadla, J. F. Lignin-based carbon fibers: Effect of synthetic polymer blending on fiber properties. *J. Polym. Environ.* **2005**, *13*, 97−105.
(78) Nowak, A. P.; Hagberg, J.; Leijonmarck, S.; Schweinebarth, H.; Baker, D.; Uhlin, A.; Tomani, P.; Lindbergh, G. Lignin-based carbon fibers for renewable and multifunctional lithium-ion battery electrodes. *Holzforschung* **2018**, *72*, 81−90.
(79) Qin, W.; Kadla, J. F. Effect of organoclay reinforcement on lignin-based carbon fibers. *Ind. Eng. Chem. Res.* **2011**, *50*, 12548−12555.
(80) Byrne, N.; Setty, M.; Blight, S.; Tadros, R.; Ma, Y.; Sixta, H.; Hummel, M. Cellulose-Derived Carbon Fibers Produced via a Continuous Carbonization Process: Investigating Precursor Choice and Carbonization Conditions. *Macromol. Chem. Phys.* **2016**, *217*, 2517−2524.
(81) Zhang, M.; Ogale, A. A. Carbon fibers from dry-spinning of acetylated softwood kraft lignin. *Carbon* **2014**, *69*, 626−629.
(82) Kim, M. S.; Lee, D. H.; Kim, C. H.; Lee, Y. J.; Hwang, J. Y.; Yang, C.-M.; Kim, Y. A.; Yang, K. S. Shell−core structured carbon fibers via melt spinning of petroleum-and wood-processing waste blends. *Carbon* **2015**, *85*, 194−200.

https://dx.doi.org/10.1021/acs.biomac.0c01117
Biomacromolecules 2020, 21, 4326−4335